

# Score-based generative diffusion with “active” correlated noise sources

Alexandra Lamtyugina,<sup>1</sup> Agnish Kumar Behera,<sup>1</sup> Aditya Nandy,<sup>1,2</sup>

Carlos Floyd,<sup>1,2</sup> and Suriyanarayanan Vaikuntanathan<sup>1,2,\*</sup>

<sup>1</sup>*Department of Chemistry, University of Chicago, Chicago, IL, 60637*

<sup>2</sup>*The James Franck Institute, University of Chicago, Chicago, IL, 60637*

Diffusion models exhibit robust generative properties by approximating the underlying distribution of a dataset and synthesizing data by sampling from the approximated distribution. In this work, we explore how the generative performance may be modulated if noise sources with temporal correlations—akin to those used in the field of active matter—are used for the destruction of the data in the forward process. Our numerical and analytical experiments suggest that the corresponding reverse process may exhibit improved generative properties.

## I. INTRODUCTION

In recent years the scientific and public interest in generative modeling has dramatically increased [1–3]. Generative modeling techniques allow the sampling of complex, high-dimensional distributions from large datasets without explicit knowledge of the distribution’s analytical form. Image, video, and music generation tools such as DALL-E [4] have captured the public attention, while scientific aims have been advanced through new techniques for sampling of molecular structures and conformations to progress drug discovery and bioinformatics [5, 6], sampling of Lagrangian turbulence to study fluid mechanics [7], and sampling of geological landscapes to study geophysics [8], to name just a few examples. Due to their wide-spread popularity, much research effort has been devoted to improving the trainability, evaluation speed, and expressivity of generative models [9–15]. Here, we take inspiration from the field of active matter [16] and propose a new variant of generative modeling that provides an orthogonal axis along which to tune hyperparameters and optimize training and sampling efficiency.

A broad class of generative models used in many application domains is the class of score-based diffusion models [17]. In these models, samples from the training dataset are first transformed into multidimensional Gaussian distributions (with variance specified by the hyperparameters of the model) through a process analogous to overdamped Brownian diffusion in a harmonic potential [2, 18]. During this “forward” phase, a neural network (NN) is trained to learn the distribution’s score function, which encodes information about how the data samples are progressively transformed into Gaussian white noise. Then, in a reverse-time diffusion process, new samples are constructed by effectively reversing the forward diffusion process using the trained neural network, through trajectories starting from points in the multidimensional Gaussian distribution [17]. This process, based on standard stochastic calculus techniques

with inspiration from non-equilibrium thermodynamics [2], is remarkably effective at parameterizing the unknown target distribution from which the training samples are drawn. Combined with machine learning architectures such as U-nets, this approach can produce new samples from a high-dimensional target distributions (e.g., images) that are strikingly similar to the original data [19, 20].

Despite the success of diffusion models, there is little reason *a priori* to expect that the simplistic setting of overdamped Brownian dynamics provides in all cases the optimal physical model on which to base the diffusion process. Altering the physical model of diffusion can provide a rich and potentially crucial set of hyperparameters, orthogonal to the standard ones such as neural network width, depth, and learning rate, that can allow for improved performance. To this end, some research effort has focused on constructing analogous diffusion models using, for example, critically-damped Langevin dynamics (CLD) [21] and even electrodynamics [22], with promising results. Here, we add to this line of development by basing our physical diffusion process on *active matter systems*. Specifically, we introduce active (exponentially time-correlated) noise into the forward dynamics of generative diffusion models, replacing the Gaussian white noise. We find that this type of noise, in many cases, leads to better generative properties compared with existing schemes. The correlation time of the active noise represents a new hyperparameter which can be tuned to optimize training and sampling efficiency for different data distributions.

This paper is organized as follows. In Sec. II, we introduce the analytical theory of reverse-time diffusion in the presence of active noise-assisted forward process. In Sec. III we present the various datasets to which we apply our novel diffusion scheme and analyze its performance. Finally, in Sec. IV we propose possible mechanisms through which the correlated noise sources might be helping improve the generative properties of the diffusion process.

\* svaikunt@uchicago.edu

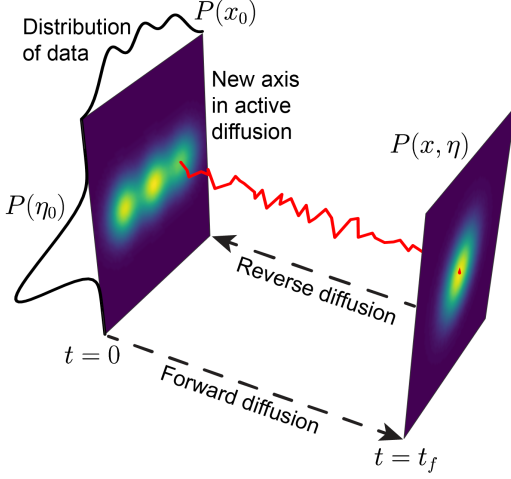


**FIG. 1:** Schematic for the forward and backward diffusion processes. Active diffusion adds a new axis coupled to the data axis along which the diffusion process is carried out. During the forward process, each of the data points is associated with a new degree of freedom,  $\eta$ , which helps in destroying the structure of the data.

## II. REVERSE-TIME DIFFUSION IN THE PRESENCE OF ACTIVE NOISE

We first review one of the standard generative diffusion frameworks. We will refer to this as “passive” diffusion [19], and it is equivalent to the diffusion process described in Ref. [17]. In the passive forward process a given data distribution is evolved according to the following equation of motion,

$$\dot{\mathbf{x}} = -k\mathbf{x} + \boldsymbol{\xi}(t) \quad (2.1)$$

where  $\mathbf{x}$  is the  $d$ -dimensional data point and the noise  $\boldsymbol{\xi}(t)$  has the properties  $\langle \xi_i(t) \rangle = 0$  and  $\langle \xi_i(t)\xi_j(t') \rangle = 2T\delta_{ij}\delta(t-t') \forall i, j$ . This evolution systematically destroys the correlations in the data. The temperature  $T$  and stiffness  $k$  are hyperparameters that set the timescale of relaxation and the width of the eventual multidimensional Gaussian distribution, with mean 0 and variance  $T/k$ , the system settles into. The reverse diffusion process then reconstructs the data distribution back from the Gaussian distribution, with dynamics given by

$$-\dot{\mathbf{x}} = -\mathbf{x} + 2T\mathcal{F}(\mathbf{x}; t) + \boldsymbol{\xi}(t) \quad (2.2)$$

where  $\mathcal{F}(\mathbf{x}; t) \equiv \nabla_{\mathbf{x}} \log P(\mathbf{x}, t)$  is the score function which helps guide the reverse trajectories to the original distribution [18]. The exact form of the score function  $\mathcal{F}(\mathbf{x}, t)$  depends on the initial distribution from which the data is drawn. For most distributions, the score function cannot be calculated analytically and is instead approximated from data using neural network models. The loss function  $\mathcal{L}$  guiding the construction of the neural network model is given as a mean-squared error between the true score function and that calculated from training data. Following [19], an expression for  $\mathcal{L}$  can be derived

using

$$\frac{\partial \log P(\mathbf{x}, t)}{\partial x_i} = -\frac{x_i - \langle x_{0,i} \rangle_{P(\mathbf{x}_0|\mathbf{x})} e^{-kt}}{\Delta_t} \quad (2.3)$$

where  $\Delta_t \equiv \frac{T}{k}(1 - e^{-2kt})$  and  $\mathbf{x}_0$  is the data configuration at  $t = 0$ . Using this, we can construct a mean-squared-error loss function

$$\mathcal{L} = \int d\mathbf{x} P(\mathbf{x}, t) \|S_{\mathbf{w}}(\mathbf{x}) - \mathcal{F}(\mathbf{x}, t)\|^2 \quad (2.4)$$

$$= \mathbb{E}_{P(\mathbf{x}, \mathbf{x}_0)} \left[ \left\| S_{\mathbf{w}}(\mathbf{x}) + \frac{\mathbf{x} - \langle \mathbf{x}_0 \rangle_{P(\mathbf{x}_0|\mathbf{x})} e^{-kt}}{\Delta_t} \right\|^2 \right] \quad (2.5)$$

Here,  $S_{\mathbf{w}}(\mathbf{x})$  is the neural network model for the score function, and  $\mathbf{w}$  denotes the various tunable parameters (weights) of the neural network, which are optimized using stochastic gradient descent algorithms.

Building on this existing framework, we construct our “active” generative diffusion process. Under the influence of active noise, the forward process is:

$$\dot{\mathbf{x}} = -k\mathbf{x} + \boldsymbol{\eta}(t) + \boldsymbol{\xi}_1(t) \quad (2.6)$$

$$\dot{\boldsymbol{\eta}} = -\frac{\boldsymbol{\eta}}{\tau} + \boldsymbol{\xi}_2(t) \quad (2.7)$$

$$\langle \xi_{1,i}(t) \rangle = 0, \quad \langle \xi_{2,i}(t) \rangle = 0, \quad (2.8)$$

$$\langle \xi_{1,i}(t)\xi_{1,j}(t') \rangle = 2T_p\delta_{ij}\delta(t-t') \forall i, j \quad (2.9)$$

$$\langle \xi_{2,i}(t)\xi_{2,j}(t') \rangle = \frac{2T_a}{\tau^2}\delta_{ij}\delta(t-t') \forall i, j \quad (2.10)$$

As shown in the schematic of Fig. 1, every “data” degree of freedom,  $\mathbf{x}$ , gets an “active” degree of freedom,  $\boldsymbol{\eta}$  associated with its evolution. In essence the dimension of the system is increased from  $d$  to  $2d$  where  $d$  is the dimension of the data. In Sec. A1 we show that the reverse diffusion for this process is given by

$$-\dot{\mathbf{x}} = -k\mathbf{x} + \boldsymbol{\eta} + 2T_p\mathcal{F}_{\mathbf{x}}(\mathbf{x}, \boldsymbol{\eta}; t) + \boldsymbol{\xi}_1(t) \quad (2.11)$$

$$-\dot{\boldsymbol{\eta}} = -\frac{\boldsymbol{\eta}}{\tau} + \frac{2T_a}{\tau^2}\mathcal{F}_{\boldsymbol{\eta}}(\mathbf{x}, \boldsymbol{\eta}; t) + \boldsymbol{\xi}_2(t) \quad (2.12)$$

where  $\mathcal{F}_{\mathbf{x}}(\mathbf{x}, \boldsymbol{\eta}; t) \equiv \nabla_{\mathbf{x}} \log P(\mathbf{x}, \boldsymbol{\eta}; t)$  and  $\mathcal{F}_{\boldsymbol{\eta}}(\mathbf{x}, \boldsymbol{\eta}; t) \equiv \nabla_{\boldsymbol{\eta}} \log P(\mathbf{x}, \boldsymbol{\eta}; t)$  are the score functions for this process.

As in the passive case, one can construct the loss function for training the neural network as

$$\mathcal{L} = \int d\mathbf{x} d\boldsymbol{\eta} P(\mathbf{x}, \boldsymbol{\eta}; t) [\|S_{\mathbf{w}}^{(\mathbf{x})}(\mathbf{x}, \boldsymbol{\eta}) - \mathcal{F}_{\mathbf{x}}(\mathbf{x}, \boldsymbol{\eta}; t)\|^2 + \|S_{\mathbf{w}}^{(\boldsymbol{\eta})}(\mathbf{x}, \boldsymbol{\eta}) - \mathcal{F}_{\boldsymbol{\eta}}(\mathbf{x}, \boldsymbol{\eta}; t)\|^2]. \quad (2.13)$$

Here  $S^{(\mathbf{x})}$  and  $S^{(\boldsymbol{\eta})}$  are two different neural networks used for approximating the score in  $\mathbf{x}$  and the score in  $\boldsymbol{\eta}$ , respectively. We derive the forms of  $\mathcal{F}_{\mathbf{x}}(\mathbf{x}, \boldsymbol{\eta}; t)$  and  $\mathcal{F}_{\boldsymbol{\eta}}(\mathbf{x}, \boldsymbol{\eta}; t)$  in Sec. A1. For the purpose of directly comparing the passive case to the active case, we set  $T_p = 0$  in all the active simulations. This choice leads to training of only the neural network for  $\mathcal{F}_{\boldsymbol{\eta}}(\mathbf{x}, \boldsymbol{\eta}; t)$  since  $\mathcal{F}_{\mathbf{x}}(\mathbf{x}, \boldsymbol{\eta}; t)$  becomes irrelevant for the reverse process.

We note that a similar approach of expanding the dimensionality through additional degrees of freedom is taken in [21], which presents an underdamped pas-

sive Brownian diffusion process (referred to as critically-damped Langevin diffusion, CLD). In that case, destructive noise is not added to the data directly but instead to velocity degrees of freedom. Because of this similarity, we build upon the numerical implementation provided by Ref. [21] to diffuse data according to the active process which we present in this paper. Implementation details are discussed in Sec. A2. In the next section, we discuss various numerical experiments where we compare the performance of passive and active generative diffusion models. Comparisons to results of the CLD [21] are included and discussed in the SI.

### III. CHARACTERIZATION OF THE PASSIVE AND ACTIVE SCORE FUNCTIONS

The performance of generative diffusion is governed by the ability to accurately learn the score function and evolve the equations of motion of the reverse diffusion process. In this section, we examine the effects of approximating the score function on the performance of passive and active diffusion. First, we examine diffusion performance on a target distribution for which the analytic form of the score is known. Then, we numerically approximate the score function with a multi-layer perceptron (MLP) NN from data and examine the effects of discretization of the learned score function in the sampling process of reverse diffusion. Details on the NN architecture and numerical implementation are in Sec. A2.

#### A. Gaussian mixture 2D distribution: analytic score vs. score modeled by a neural network

The score function for simple distributions such as a mixture of Gaussian peaks can be expressed analytically. The analytical score functions for such distributions can be used to compare the performance of passive and active diffusion without needing to account for the learning performance of neural networks, since in this case the score functions are known exactly and do not need to be inferred from training data. In these numerical experiments, we investigate the performance with respect to the time step size for the reverse diffusion process. The time step size is given by  $dt = t_f/n$ , where  $t_f$  is the total time of a trajectory and  $n$  is the number of synthesis steps. For all diffusion trajectories presented here,  $t_f = 1$ .

The Gaussian mixture distribution is a typical simple distribution to test the performance of the neural networks in generating the reverse diffusion process. The score functions of Gaussian distributions have an exact analytic form. The data distribution we generate is given by,

$$P_0(\mathbf{x}_0) \propto \sum_{\alpha} \frac{p_{\alpha}}{\prod_i \sqrt{h_i^{\alpha}}} \exp \left( - \sum_i \frac{(x_{0,i} - \mu_i^{\alpha})^2}{2h_i^{\alpha}} \right) \quad (3.1)$$

where  $i$  denotes the dimension of the data,  $\mu_i^{\alpha}$  and  $h_i^{\alpha}$  describe the location of the mean and the corresponding variance, respectively, of the  $\alpha^{th}$  Gaussian in  $i^{th}$  dimension, and  $p_{\alpha}$  represents the weight given to each of the Gaussian peaks in the mixture. The details of the derivation of the score functions for the passive and active processes are provided in Sec. A3.

We use a distribution where 9 Gaussians are spaced in a diamond formation (see Sec. A4 for parameters used to generate the distributions). We perform reverse diffusion using the analytical score function and the score function learned by a NN (Fig. 2).

Using the analytical score function for the reverse process, Fig. 2a shows that for large time step size ( $dt = 0.1$  and  $dt = 0.01$ ), the active process performs better than its passive counterpart. If the time step is small enough ( $dt = 0.002$ ), both passive and active diffusion achieve comparable performance and both are able to faithfully reproduce the target distribution. When we use neural networks to learn the score function numerically for the same data distribution (Fig. 2b), passive and active processes show similar trends as in the analytical case in Fig. 2a, though the overall performance is lower than when the analytical score is used. We note that here, for exact comparison between the analytical case and the case with neural networks, we turn off denoising in the final step of the reverse diffusion process. Generally for passive diffusion processes, the last step of reverse diffusion is carried out with only the drift term and the noise term is set to zero. This last denoising step has been observed to improve FID scores in image datasets [23]. In our case of active reverse diffusion, the denoising step has no effect as the denoising is applied to the  $\boldsymbol{\eta}$  dimension. In passive reverse diffusion, however, the denoising step affects the quality of generated data since the denoising is applied to the data directly. Additional details are provided in Sec. A2 C.

#### B. Distributions with unknown score functions

We next test the performance of passive and active diffusion on 2D distributions with less symmetry and more multi-scale structure than the diamond of Gaussians. To compare passive and active processes for a chemical system, we consider the protein alanine dipeptide, a small model benchmark system that can be studied at long timescales (Fig. 3a). We started with the geometry of the alanine dipeptide from a previous benchmarking study [24]. The details of the training data generation procedure are given in Sec. A5. For this sampling, we computed the Ramachandran dihedral angles ( $\phi, \psi$ ) for all conformations. Based on the energy landscape of the alanine dipeptide, three major conformations [25] ( $\alpha_R$  [ $(\phi, \psi) = (-60^{\circ}, -45^{\circ})$ ],  $P_{II}$  [ $(\phi, \psi) = (-75^{\circ}, 145^{\circ})$ ],  $C_5$  [ $(\phi, \psi) = (-180^{\circ}, 180^{\circ})$ ]) emerge from the molecular dynamics simulation, with other conformations sampled less frequently. We use generative diffusion to resample

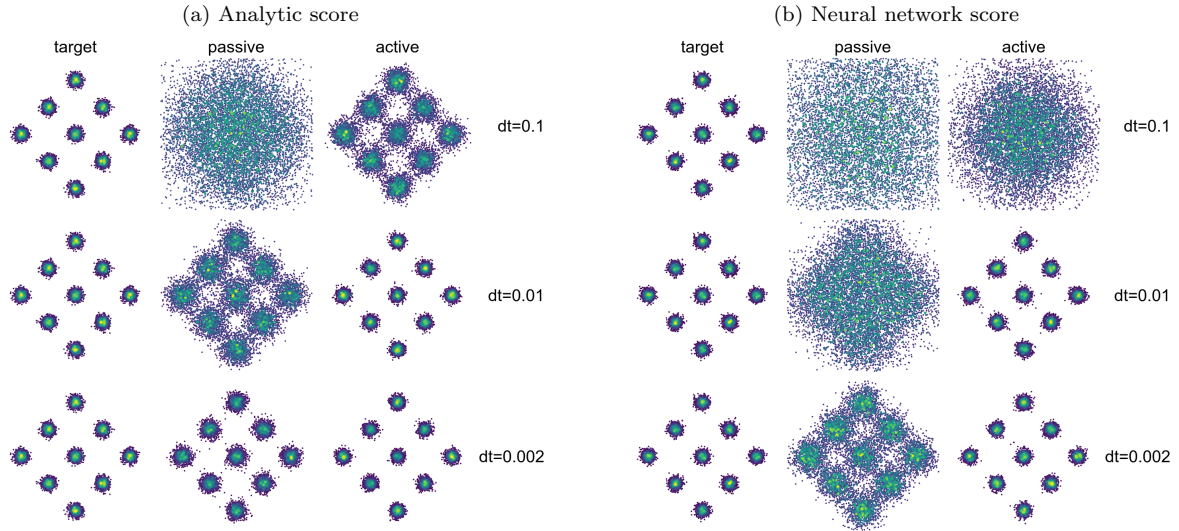


**FIG. 2:** Generation of samples in Gaussian mixture distribution via reverse diffusion with analytical (a) scores and scores learned with a neural network from training data (b). Each scatter plot contains 10,000 2D samples, colored by sample density for visual clarity (higher densities are indicated by green points and lower densities by purple). (a) Active diffusion outperforms passive case for larger  $dt$ , the time step size of the reverse diffusion trajectory. As the number of time steps of the reverse process increases, the performance of passive diffusion becomes comparable to that of active diffusion. For very small  $dt$ , both passive and active diffusion faithfully reproduce the target distribution. (b) Passive diffusion initially performs better at large  $dt$ , but as the sampling step size is decreased, active diffusion begins to outperform passive diffusion. While passive diffusion has the initial advantage at large  $dt$ , it is unable to reproduce the target distribution as accurately as active diffusion at  $dt = 0.002$ .

the two dimensional  $(\phi, \psi)$  landscape. Relative to passive diffusion, active diffusion is able to better reproduce the landscape sampled during molecular dynamics. In particular, the distribution of the Ramachandran dihedral angles of the  $C_5$  conformation are better reproduced by active diffusion relative to passive diffusion. While the positions of the  $\alpha_R$  and  $P_{II}$  angle distributions are also reproduced by both models, the separation between them is more evident in the samples generated by the active model in the same number of iterations.

We also study a data distribution consisting of overlapping Swiss rolls (Fig. 3b) to test the method on a toy model distribution for which the analytical form of the score function is not known. An important feature of this example is that the true distribution has structure at multiple length scales: both the position of the rolls and their interior structures need to be captured by the generative diffusion model. We use neural networks to learn the score functions, and, as in the Gaussian mixture model example, we observe that active diffusion outperforms passive diffusion (Fig. 2b). Additional results for this and other toy models can be found in in Sec. A4. We observe that the passive process is unable to generate the target distribution for all values of time step size and for the entire range of iterations we have considered in Fig. A4, whereas the active process succeeds in accurately resolving both scales of the target distribution.

### C. Active generative diffusion better recreates distributions and correlations of an Ising model

The data distributions considered thus far have been two-dimensional. We next test the performance of active diffusion on high-dimensional image-like data, through snapshots of Ising lattices. For this section, we use datasets generated by running Markov chain Monte Carlo (MCMC) simulations for the 2D Ising model on a 32-by-32 lattice. We generated lattice configurations at multiple temperatures ( $T = 1$  and  $T = 2$ ), below the critical point of the 2D Ising model ( $T_c = 2.269$ ) and attempted to recreate these data using the active and passive generative models. The correlations and domain distributions of the Ising model are controlled by the temperature.

To compare the performance of various networks, we use a coarse-grained metric. For every dataset, both training and diffusion-generated, we use uniform spatial convolution filters of size  $l \times l$  where  $l$  ranges from 0 to  $\frac{L}{2}$  with  $L = 32$  (the lattice edge length). The convolution is followed by taking the absolute value for every coarse-grained position, and the average is then computed for the lattice. This provides us with a coarse-grained “magnetization” metric. The ensemble average is then computed over the specific dataset. Intuitively, this provides us with a measure of the abundance of different clusters of all-“up” or all-“down” spins in the system. The difference in performance between passive and active diffusion processes is most evident for low numbers of training it-



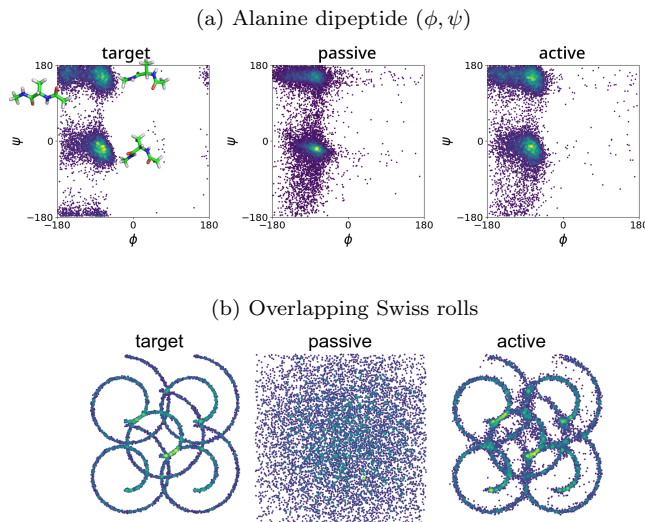


**FIG. 3:** (a) Ramachandran plots  $(\phi, \psi)$  in degrees for  $1 \mu\text{s}$  of molecular dynamics sampling for a water-solvated alanine dipeptide (left) and corresponding diffusion generated samples with passive (center), and active ( $\tau = 0.5$ ) (right). (b) Generation of samples for a 2D distribution of multiple overlapping Swiss rolls via reverse diffusion with the score function approximated by a neural network.

eration (e.g. 100 as in Fig. 4). For  $T = 1$ , active diffusion more accurately captures the Ising conformations. At Ising lattice temperature  $T = 2$ , active diffusion still has an advantage, albeit not as dramatically, over passive diffusion. In Sec. A7 we illustrate the evolution of the quality of the synthesized samples as the number of training iterations is increased.

#### IV. DISCUSSION

Overall, for a wide variety of distributions, we observe that active diffusion outperforms passive diffusion when the features of the distribution are shorter than the typical length scale of diffusion. We speculate this could happen for a variety of reasons.

The score function learned in the passive process typically has a faster rate of change when compared with the score function learned in the active process. This is due to the extra time scale  $\tau$  introduced in the active process. The spatial Fourier components decay more slowly at the beginning of the forward process for the active case when compared to the passive case (see Sec. A6). This feature might help the neural network learn the score function more effectively in fewer steps in the active case. In numerical implementation with finite time steps, the active score function with slower temporal variation seems to outperform the passive score function. Next, following Ref [21], we expect that the score function of the active process has a lower functional complexity than the score function of the passive process. Indeed, the score

function of the active process is mainly represented in terms of the  $\eta$  degrees of freedom which may be easier to encode than the full data distribution. We compare the performance of active diffusion to the Critically-damped Langevin Diffusion (CLD) presented in Ref. [21] in Sec. A4, A5 and A7.

Next, the initial sampling from the standard multi-dimensional distribution at the beginning of the “backward” diffusion or generation process is exact only in the limit where the number of samples approaches infinity, which is obviously implausible in practice. This error due to finite sampling could lead to the sampled distribution being further away from the target distribution. It has recently been theoretically shown that this deviation from the target distribution increases with entropy-production that accompanies the generation process [26, 27]. The active process may ensure better sampling from the active degrees augmented Gaussian distribution and also may lead to lower entropy production rates.

Even with the analytic score function, the reverse trajectories for the generation process are still computed numerically by discretizing the trajectory into finite steps of length  $dt$ . With an infinitely small  $dt$ , reverse diffu-

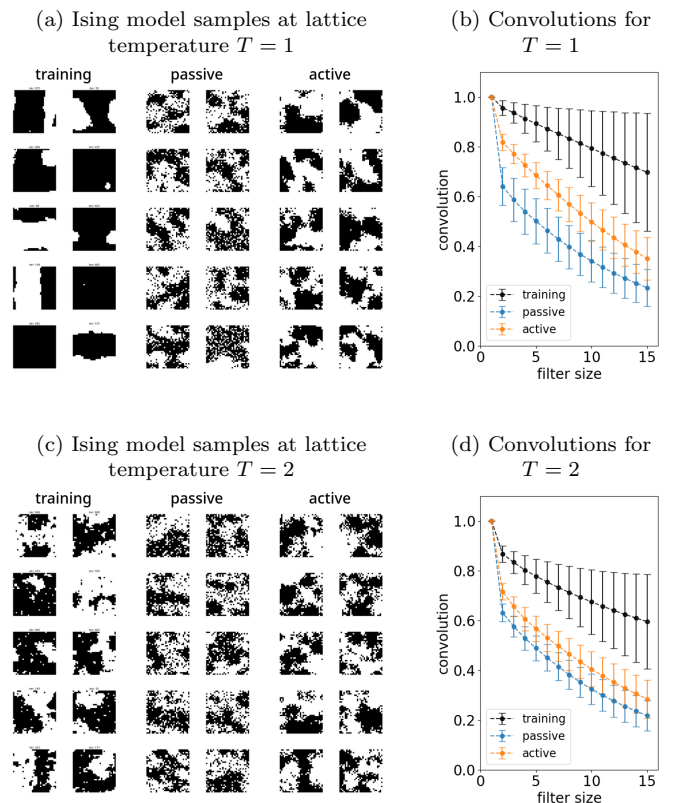


**FIG. 4:** Training and diffusion (passive and active) samples after 100 training iterations at  $T = 1$  (a) and  $T = 2$  (c). Diffusion samples were generated with the ODE sampler with adaptive  $dt$ . Convolution for  $T = 1$  (b) and  $T = 2$  (d). Calculated convolutions for samples generated with active diffusion more closely resemble the training data.

sion with the analytic form of the score (regardless of its underlying diffusion mechanism) will easily transform a white noise distribution into the target distribution encoded by the score function. By varying the  $dt$  used to sample the analytic score over the course of the reverse diffusion trajectory, we can explore whether the time-dependent score function encodes the information required to “denoise” a sample uniformly across the duration of the whole process. Compared to passive diffusion, active diffusion more effectively generates the target distribution even at large  $dt$  (0.1 and 0.01) as shown in Fig. 2a. This suggests that the information required to generate the target is more uniformly encoded in the active score function along the diffusion time axis, allowing it to perform reasonably well even with sparse sampling.

Finally, following Ref. [20], we can show that with active noise, it takes a shorter amount of time for trajectories in the reverse process to choose their primary class of data. For instance, in the case of Gaussian mixture model, active diffusion will choose one of the Gaussian basins to fall into sooner than in passive diffusion. The details of the calculation are provided in Sec. A8. Comparing the expression for speciation time with active noise (see Eq. (A11)) to the expression for the passive case,  $t_s^p = \frac{1}{2} \log\left(\frac{\max_\lambda(C_0)}{T_p}\right)$ , where  $T_p$  is the passive temperature, we observe that for a fixed target distribution and for the same passive and active temperature ( $T_p = T_a$ ),  $t_s^a > t_s^p$  (here the time,  $t$ , is being measured in the forward diffusion process i.e.  $t = 0$  corresponds to the data distribution at the start of the forward process). Thus for the reverse diffusion process, the speciation hap-

pens faster in the active case when compared to passive case. Faster speciation would imply that more time can be spent sampling the various peaks in the data distribution, which could lead to better fine-scale resolution in the generated configurations.

Our results present numerical evidence that the active generative diffusion process has in some cases an improved training and sampling performance compared to the diffusion processes previously employed in score-based generative modeling. We leave a full theoretical treatment of this and other physics-inspired diffusion processes to future work. We hope this work can encourage exploring how dynamics that have been extensively studied in the context of physical systems can be leveraged to improve the performance of machine learning techniques.

## V. ACKNOWLEDGMENTS

SV, CF and AL acknowledge support by the National Institute of General Medical Sciences of the NIH under Award No. R35GM147400. AKB acknowledges support from a fellowship from the Department of Chemistry at the University of Chicago. AN gratefully acknowledges support from the Eric and Wendy Schmidt AI in Science Postdoctoral Fellowship, a Schmidt Sciences program. We also acknowledge helpful initial discussions with Pratyush Tiwary, helpful discussions with Lorenzo Orecchia, and helpful comments by Aaron Dinner on an initial version of this manuscript.

- 
- [1] Ling Yang, Zhilong Zhang, Yang Song, Shenda Hong, Runsheng Xu, Yue Zhao, Wentao Zhang, Bin Cui, and Ming-Hsuan Yang. Diffusion models: A comprehensive survey of methods and applications. *ACM Computing Surveys*, 56(4):1–39, 2023.
  - [2] Jascha Sohl-Dickstein, Eric Weiss, Niru Maheswaranathan, and Surya Ganguli. Deep unsupervised learning using nonequilibrium thermodynamics. In *International conference on machine learning*, pages 2256–2265. PMLR, 2015.
  - [3] Jonathan Ho, Ajay Jain, and Pieter Abbeel. Denoising diffusion probabilistic models. *Advances in neural information processing systems*, 33:6840–6851, 2020.
  - [4] Aditya Ramesh, Mikhail Pavlov, Gabriel Goh, Scott Gray, Chelsea Voss, Alec Radford, Mark Chen, and Ilya Sutskever. Zero-shot text-to-image generation. (arXiv:2102.12092), February 2021. arXiv:2102.12092 [cs].
  - [5] Camille Bilodeau, Wengong Jin, Tommi Jaakkola, Regina Barzilay, and Klavs F Jensen. Generative models for molecular discovery: Recent advances and challenges. *Wiley Interdisciplinary Reviews: Computational Molecular Science*, 12(5):e1608, 2022.
  - [6] Yihang Wang, Lukas Herron, and Pratyush Tiwary. From data to noise to data for mixing physics across temperatures with generative artificial intelligence. *Proceedings of the National Academy of Sciences*, 119(32):e2203656119, August 2022.
  - [7] Tim Whittaker, Romuald A Janik, and Yaron Oz. Turbulence scaling from deep learning diffusion generative models. *Journal of Computational Physics*, 514:113239, 2024.
  - [8] J. Lochner, J. Gain, S. Perche, A. Peytavie, E. Galin, and E. Guérin. Interactive authoring of terrain using diffusion models. *Computer Graphics Forum*, 42(7):e14941, October 2023.
  - [9] Diederik Kingma, Tim Salimans, Ben Poole, and Jonathan Ho. Variational diffusion models. *Advances in neural information processing systems*, 34:21696–21707, 2021.
  - [10] Tero Karras, Miika Aittala, Timo Aila, and Samuli Laine. Elucidating the design space of diffusion-based generative models. *Advances in neural information processing systems*, 35:26565–26577, 2022.
  - [11] Yu Cao, Jingrun Chen, Yixin Luo, and Xiang Zhou. Exploring the optimal choice for generative processes in diffusion models: Ordinary vs stochastic differential equations. *Advances in Neural Information Processing Systems*, 36:33420–33468, 2023.

- [12] René Haas, Inbar Huberman-Spiegelglas, Rotem Mulyoff, Stella Graßhof, Sami S Brandt, and Tomer Michaeli. Discovering interpretable directions in the semantic latent space of diffusion models. In *2024 IEEE 18th International Conference on Automatic Face and Gesture Recognition (FG)*, pages 1–9. IEEE, 2024.
- [13] Belinda Tzen and Maxim Raginsky. Theoretical guarantees for sampling and inference in generative models with latent diffusions. In *Conference on Learning Theory*, pages 3084–3114. PMLR, 2019.
- [14] Yu-Hui Chen, Raman Sarokin, Juhyun Lee, Jiuqiang Tang, Chuo-Ling Chang, Andrei Kulik, and Matthias Grundmann. Speed is all you need: On-device acceleration of large diffusion models via gpu-aware optimizations. In *Proceedings of the IEEE/CVF Conference on Computer Vision and Pattern Recognition*, pages 4651–4655, 2023.
- [15] Hao Phung, Quan Dao, and Anh Tran. Wavelet diffusion models are fast and scalable image generators. In *Proceedings of the IEEE/CVF conference on computer vision and pattern recognition*, pages 10199–10208, 2023.
- [16] Étienne Fodor, Cesare Nardini, Michael E Cates, Julien Tailleur, Paolo Visco, and Frédéric Van Wijland. How far from equilibrium is active matter? *Physical review letters*, 117(3):038103, 2016.
- [17] Yang Song, Jascha Sohl-Dickstein, Diederik P. Kingma, Abhishek Kumar, Stefano Ermon, and Ben Poole. Score-based generative modeling through stochastic differential equations. (arXiv:2011.13456), February 2021. arXiv:2011.13456 [cs, stat].
- [18] Brian DO Anderson. Reverse-time diffusion equation models. *Stochastic Processes and their Applications*, 12(3):313–326, 1982.
- [19] Giulio Biroli and Marc Mézard. Generative diffusion in very large dimensions. *Journal of Statistical Mechanics: Theory and Experiment*, 2023(9):093402, 2023.
- [20] Giulio Biroli, Tony Bonnaire, Valentin De Bortoli, and Marc Mézard. Dynamical regimes of diffusion models. arXiv preprint arXiv:2402.18491, 2024.
- [21] Tim Dockhorn, Arash Vahdat, and Karsten Kreis. Score-based generative modeling with critically-damped langevin diffusion. arXiv preprint arXiv:2112.07068, 2021.
- [22] Yilun Xu, Ziming Liu, Max Tegmark, and Tommi Jaakkola. Poisson flow generative models. (arXiv:2209.11178), October 2022. arXiv:2209.11178 [cs].
- [23] Alexia Jolicoeur-Martineau, Ke Li, Rémi Piché-Taillefer, Tal Kachman, and Ioannis Mitliagkas. Gotta go fast when generating data with score-based models. (arXiv:2105.14080), May 2021. arXiv:2105.14080 [cs].
- [24] Feliks Nüske, Hao Wu, Jan-Hendrik Prinz, Christoph Wehmeyer, Cecilia Clementi, and Frank Noé. Markov state models from short non-equilibrium simulations—Analysis and correction of estimation bias. *The Journal of Chemical Physics*, 146(9):094104, 03 2017.
- [25] Christoph F. Weise and James C. Weisshaar. Conformational analysis of alanine dipeptide from dipolar couplings in a water-based liquid crystal. *The Journal of Physical Chemistry B*, 107(14):3265–3277, 2003.
- [26] Kotaro Ikeda, Tomoya Uda, Daisuke Okanohara, and Sosuke Ito. Speed-accuracy trade-off for the diffusion models: Wisdom from nonequilibrium thermodynamics and optimal transport. arXiv preprint arXiv:2407.04495, 2024.
- [27] Akhil Premkumar. Neural entropy. arXiv preprint arXiv:2409.03817, 2024.
- [28] Arash Vahdat, Karsten Kreis, and Jan Kautz. Score-based generative modeling in latent space. *Advances in neural information processing systems*, 34:11287–11302, 2021.
- [29] H.J.C. Berendsen, D. van der Spoel, and R. van Drunen. Gromacs: A message-passing parallel molecular dynamics implementation. *Computer Physics Communications*, 91(1):43–56, 1995.
- [30] Mark James Abraham, Teemu Murtola, Roland Schulz, Szilárd Páll, Jeremy C. Smith, Berk Hess, and Erik Lindahl. Gromacs: High performance molecular simulations through multi-level parallelism from laptops to supercomputers. *SoftwareX*, 1-2:19–25, 2015.
- [31] Yong Duan, Chun Wu, Shibusish Chowdhury, Mathew C. Lee, Guoming Xiong, Wei Zhang, Rong Yang, Piotr Cieplak, Ray Luo, Taisung Lee, James Caldwell, Junmei Wang, and Peter Kollman. A point-charge force field for molecular mechanics simulations of proteins based on condensed-phase quantum mechanical calculations. *Journal of Computational Chemistry*, 24(16):1999–2012, 2003.
- [32] William L. Jorgensen, Jayaraman Chandrasekhar, Jeffrey D. Madura, Roger W. Impey, and Michael L. Klein. Comparison of simple potential functions for simulating liquid water. *The Journal of Chemical Physics*, 79(2):926–935, 07 1983.
- [33] Tom Darden, Darrin York, and Lee Pedersen. Particle mesh Ewald: An Nlog(N) method for Ewald sums in large systems. *The Journal of Chemical Physics*, 98(12):10089–10092, 06 1993.
- [34] Giovanni Bussi, Davide Donadio, and Michele Parrinello. Canonical sampling through velocity rescaling. *The Journal of Chemical Physics*, 126(1):014101, 01 2007.
- [35] M. Parrinello and A. Rahman. Polymorphic transitions in single crystals: A new molecular dynamics method. *Journal of Applied Physics*, 52(12):7182–7190, 12 1981.

## A1. DERIVATION FOR ACTIVE REVERSE DIFFUSION

The forward process for active diffusion is given as

$$\dot{\mathbf{x}} = -k\mathbf{x} + \boldsymbol{\eta}(t) + \boldsymbol{\xi}_1(t), \quad (\text{A1})$$

$$\dot{\boldsymbol{\eta}} = -\frac{\boldsymbol{\eta}}{\tau} + \boldsymbol{\xi}_2(t), \quad (\text{A2})$$

$$\langle \xi_{1,i}(t) \rangle = 0, \quad \langle \xi_{2,i}(t) \rangle = 0, \quad (\text{A3})$$

$$\langle \xi_{1,i}(t) \xi_{1,j}(t') \rangle = 2T_p \delta_{ij} \delta(t - t') \forall i, j \quad (\text{A4})$$

$$\langle \xi_{2,i}(t) \xi_{2,j}(t') \rangle = \frac{2T_a}{\tau^2} \delta_{ij} \delta(t - t') \forall i, j. \quad (\text{A5})$$

The initial condition for the forward process is the joint distribution between the data degrees of freedom ( $\mathbf{x}$ ) and the corresponding active degrees of freedom ( $\boldsymbol{\eta}$ ), and it is constructed as

$$P_0(\mathbf{x}, \boldsymbol{\eta}) = P_0(\mathbf{x})P_0(\boldsymbol{\eta}) \quad (\text{A6})$$

$$P_0(\boldsymbol{\eta}) \propto \exp\left(-\frac{\tau}{2T_a} \boldsymbol{\eta} \cdot \boldsymbol{\eta}\right) \quad (\text{A7})$$

where  $P_0(\mathbf{x})$  is the distribution from which the data is drawn. With these initial conditions,  $P(\mathbf{x}, \boldsymbol{\eta}, t)$  is given by

$$P(\mathbf{x}, \boldsymbol{\eta} | \mathbf{x}_0, \boldsymbol{\eta}_0; t) \propto \exp\left(-\frac{\vec{X}^T C^{-1} \vec{X}}{2}\right) \quad (\text{A8})$$

$$\vec{X} = \begin{pmatrix} \mathbf{x} - e^{-kt} \mathbf{x}_0 - \frac{e^{-t/\tau} - e^{-kt}}{k - \frac{1}{\tau}} \boldsymbol{\eta}_0 \\ \boldsymbol{\eta} - e^{-t/\tau} \boldsymbol{\eta}_0 \end{pmatrix} \quad (\text{A9})$$

$$C = \begin{pmatrix} m_{11} & m_{12} \\ m_{12} & m_{22} \end{pmatrix} \circ \mathbb{1}_d \quad (\text{A10})$$

$$m_{11} = \frac{1}{k} T_p (1 - a^2) + \frac{T_a}{\tau^2} \left( \frac{\tau}{kc} + \frac{1}{d^2} \left( \frac{4ab}{c} - b^2 \tau - \frac{a^2}{k} \right) \right) \quad (\text{A11})$$

$$m_{12} = \frac{T_a}{\tau c d} \left( k(1 - b^2) - \frac{1}{\tau} (1 + b^2 - 2ab) \right) \quad (\text{A12})$$

$$m_{22} = \frac{T_a}{\tau} (1 - b^2) \quad (\text{A13})$$

$$a = e^{-kt}, \quad b = e^{-t/\tau}, \quad c = k + \frac{1}{\tau}, \quad d = k - \frac{1}{\tau}. \quad (\text{A14})$$

The reverse diffusion for this process is then given by

$$-\dot{\mathbf{x}} = -k\mathbf{x} + \boldsymbol{\eta} + 2T_p \mathcal{F}_{\mathbf{x}}(\mathbf{x}, \boldsymbol{\eta}, t) + \boldsymbol{\xi}_1(t) \quad (\text{A15})$$

$$-\dot{\boldsymbol{\eta}} = -\frac{\boldsymbol{\eta}}{\tau} + \frac{2T_a}{\tau^2} \mathcal{F}_{\boldsymbol{\eta}}(\mathbf{x}, \boldsymbol{\eta}, t) + \boldsymbol{\xi}_2(t) \quad (\text{A16})$$

where  $\mathcal{F}_{\mathbf{x}}(\mathbf{x}, \boldsymbol{\eta}, t) \equiv \nabla_{\mathbf{x}} \log P(\mathbf{x}, \boldsymbol{\eta}, t)$  and  $\mathcal{F}_{\boldsymbol{\eta}}(\mathbf{x}, \boldsymbol{\eta}, t) \equiv \nabla_{\boldsymbol{\eta}} \log P(\mathbf{x}, \boldsymbol{\eta}, t)$  are the score functions for this process.

Using Eq. (A5), we construct  $P(\mathbf{x}, \boldsymbol{\eta}; t)$  and obtain the expressions for the loss functions corresponding to the scores.

$$P(\mathbf{x}, \boldsymbol{\eta}; t) = \int P(\mathbf{x}, \boldsymbol{\eta} | \mathbf{x}_0, \boldsymbol{\eta}_0; t) P(\mathbf{x}_0, \boldsymbol{\eta}_0) d\mathbf{x}_0 d\boldsymbol{\eta}_0 \quad (\text{A17})$$

$$\mathcal{F}_{\mathbf{x}}(\mathbf{x}, \boldsymbol{\eta}; t) = \frac{-m_{22}(\mathbf{x} - a \langle \mathbf{x}_0 \rangle - \frac{a-b}{d} \langle \boldsymbol{\eta}_0 \rangle) + m_{12}(\boldsymbol{\eta} - b \langle \boldsymbol{\eta}_0 \rangle)}{\Delta_t} \quad (\text{A18})$$

$$\mathcal{F}_{\boldsymbol{\eta}}(\mathbf{x}, \boldsymbol{\eta}; t) = \frac{-m_{11}(\boldsymbol{\eta} - b \langle \boldsymbol{\eta}_0 \rangle) + m_{12}(\mathbf{x} - a \langle \mathbf{x}_0 \rangle - \frac{a-b}{d} \langle \boldsymbol{\eta}_0 \rangle)}{\Delta_t} \quad (\text{A19})$$

where  $\langle \cdot \rangle$  denotes  $\mathbb{E}_{P(\mathbf{x}_0, \boldsymbol{\eta}_0 | \mathbf{x}, \boldsymbol{\eta}; t)}[\cdot]$ .

Setting  $T_p = 0$  in the active process allows us to ignore  $\mathcal{F}_{\mathbf{x}}$  and learn only  $\mathcal{F}_{\boldsymbol{\eta}}$ . See Ref. [21] for a discussion on why  $\mathcal{F}_{\mathbf{x}}$  is more difficult to learn.

## A2. NUMERICAL IMPLEMENTATION

Here we discuss the numerical implementation of reverse diffusion process using a score objective and the architecture of the neural network used. We adapt the implementation from Ref. [21]. First, the initial data,  $(\mathbf{x}_0, \boldsymbol{\eta}_0) \sim P(\mathbf{x}_0, \boldsymbol{\eta}_0)$ ,

are perturbed in the forward process over a time interval,  $t \sim \mathcal{U}[0, t_f]$ , where  $\mathcal{U}$  is the uniform distribution and  $t_f$  is the length of time for which the forward process is run. For  $t_f \rightarrow \infty$ , the data distribution reduces to a multidimensional Gaussian distribution centered at the origin. Using these generated samples at different times, we train the neural network to minimize the score objective, a hybrid score matching objective in our case [28]. To “inform” the neural network about the structure of the score, we use a mixed score parameterization [21, 28].

### A. Extension of the CLD [21] Code

The primary difference between CLD and active diffusion is the stochastic differential equations (SDEs) defining each process. Thus, implementing active diffusion was achieved by sub-classing the existing CLD class and overriding key methods such as the SDEs of the diffusion process and the perturbation kernel functions.

The 2D alanine dipeptide toy model was implemented by loading in a file with training data and randomly drawing from the imported dataset. For diffusion on the Ising model, each training sample, a 32-by-32 pixel image with 1 channel, was generated by performing 1,000,000 MCMC sampling steps from a random initial configuration. The training data was generated to have discrete values ( $-1$  or  $+1$ ), the perturbation kernel was allowed to vary lattice sites in a continuous manner, and the final samples were discretized back to values of  $(-1, +1)$  using a cutoff of 0.

### B. Neural Network Architectures

In the toy model examples (Gaussian mixtures, Swiss rolls, and alanine dipeptide), the score was learned by a multi-layer perceptron with 4 hidden layers of 128 nodes each. The Ising lattices were treated as images with one channel, and the score was learned using a neural network with the NCSN++ architecture [17].

All simulations were performed for 1,000,000 training iterations (unless otherwise specified). For the toy models, the batch size for each iteration was 512 training samples; for Ising lattices, the batch size was 1 sample per iteration. After training, all models were used to synthesize 10,000 samples. All toy models (excepting the 2D alanine dipeptide model) used the Euler-Maruyama sampling scheme. The alanine dipeptide and Ising models used an ODE sampler with adaptive step size.

### C. Sampling

In the 2D toy model examples, we disable denoising at the last step of the sampling scheme. It was previously observed that a denoising step (in which only the drift term of the reverse SDE was applied, and not the diffusion term) improved the FID scores of generated image samples by removing noise that is otherwise undetectable by the human eye [23]. This positive effect of the last denoising step is most evident in passive diffusion and does not affect the quality of the samples generated by CLD (see Ref. [21]) or, by extension, active diffusion. We disabled denoising in toy models to be able to compare the performance of analytic and numeric score functions (Fig. 2), but retain denoising in the Ising model diffusion since it is image-like in nature.

Although we make direct comparisons of the performance of sample generation of active diffusion and CLD, we note that CLD was found to perform best using a custom sampling scheme created by the authors of the method [21]. The comparison of performance of active diffusion and CLD using this sampler is intended in future iterations of this work.

## A3. EQUATION OF MOTION FOR REVERSE ACTIVE DIFFUSION FOR MULTIPLE GAUSSIANS

The passive forward diffusion process leads to the evolution of the probability density in the following way,

$$P_t(\mathbf{x}) \propto \sum_{\alpha} \frac{p_{\alpha}}{\prod_i \sqrt{h_i^{\alpha}}} \int D x_{0,i} \exp \left( - \sum_i \left( \frac{(x_{0,i} - \mu_i^{\alpha})^2}{2h_i^{\alpha}} + \frac{(x_i - a x_{0,i})^2}{2\Delta} \right) \right) \quad (\text{A1})$$

$$= \sqrt{\Delta} \sum_{\alpha} \frac{p_{\alpha}}{\prod_i \sqrt{\Delta + h_i^{\alpha} a^2}} \exp \left( - \sum_i \frac{(x_i - a \mu_i^{\alpha})^2}{2(\Delta + a^2 h_i^{\alpha})} \right) \quad (\text{A2})$$

where  $a = e^{-kt}$ , the index  $i$  runs over the different peaks, and the index  $\alpha$  runs over the dimensions of the dataset, and  $\Delta$  is given as,  $\Delta = \frac{T}{k}(1 - e^{-2kt})$ . Thus the score function for the reverse process is given by

$$\frac{\partial \log(P_t(\mathbf{x}))}{\partial x_i} = -\frac{1}{P_t(\mathbf{x})} \sum_{\alpha} \frac{p_{\alpha}}{\Pi_j \sqrt{\Delta + h_j^{\alpha} a^2}} \frac{(x_i - a\mu_i^{\alpha})}{\Delta + a^2 h_i^{\alpha}} \exp\left(-\sum_j \frac{(x_j - a\mu_j^{\alpha})^2}{2(\Delta + a^2 h_j^{\alpha})}\right) \quad (\text{A3})$$

Following the same procedure for the active process yields

$$P_0(\mathbf{x}_0) \propto \sum_{\alpha} p_{\alpha} \prod_i \left[ \frac{1}{\sqrt{h_i^{\alpha}}} \exp\left(-\frac{(x_{0,i} - \mu_i^{\alpha})^2}{2h_i^{\alpha}}\right) \right], \quad P_0(\boldsymbol{\eta}_0) \propto \exp\left(-\frac{\boldsymbol{\eta}_0^2}{2g}\right) \quad (\text{A4})$$

$$P(\mathbf{x}, \boldsymbol{\eta} | \mathbf{x}_0, \boldsymbol{\eta}_0; t) \propto \exp\left(-\frac{\vec{X}^T C^{-1} \vec{X}}{2}\right), \quad \vec{X} = \begin{pmatrix} \mathbf{x} - a\mathbf{x}_0 - b\boldsymbol{\eta}_0 \\ \boldsymbol{\eta} - c\boldsymbol{\eta}_0 \end{pmatrix}, \quad C = \begin{pmatrix} m_{11} & m_{12} \\ m_{12} & m_{22} \end{pmatrix} \quad (\text{A5})$$

$$P_t(\mathbf{x}, \boldsymbol{\eta}) \propto \sqrt{\Delta} g^{\dim s} \sum_{\alpha} p_{\alpha} \prod_i \left( \frac{h_i^{\alpha}}{\sqrt{\Delta_{\text{eff},i}^{\alpha}}} \right) \prod_i \left( \exp\left(-\frac{k_1(x_i - a\mu_i^{\alpha})^2 - 2k_2(x_i - a\mu_i^{\alpha})\eta_i + k_{3,i}^{\alpha}\eta_i^2}{2\Delta_{\text{eff},i}^{\alpha}}\right) \right) \quad (\text{A6})$$

$$k_1 = c^2 g + m_{22}, \quad k_2 = bcg + m_{12}, \quad k_{3,i}^{\alpha} = b^2 g + a^2 h_i^{\alpha} + m_{11}, \quad \Delta_{\text{eff},i}^{\alpha} = k_1 k_{3,i}^{\alpha} - k_2^2, \quad \Delta = m_{11}m_{22} - m_{12}^2 \quad (\text{A7})$$

$$\frac{\partial \ln(P(\mathbf{x}, \boldsymbol{\eta}))}{\partial x_i} = -\frac{1}{P_t(\mathbf{x}, \boldsymbol{\eta})} \sum_{\alpha} \prod_j \left( \frac{h_j^{\alpha}}{\sqrt{\Delta_{\text{eff},j}^{\alpha}}} \right) p_{\alpha} \frac{k_1(x_i - a\mu_i^{\alpha}) - k_2\eta_i}{\Delta_{\text{eff},i}^{\alpha}} z_{\alpha} \quad (\text{A8})$$

$$\frac{\partial \ln(P(\mathbf{x}, \boldsymbol{\eta}))}{\partial \eta_i} = -\frac{1}{P_t(\mathbf{x}, \boldsymbol{\eta})} \sum_{\alpha} \prod_j \left( \frac{h_j^{\gamma}}{\sqrt{\Delta_{\text{eff},j}^{\gamma}}} \right) p_{\alpha} \frac{k_{3,i}^{\alpha}\eta_i - k_2 x_i}{\Delta_{\text{eff},i}^{\alpha}} z_{\alpha} \quad (\text{A9})$$

$$z_{\alpha} = \exp\left(-\sum_r \left( \frac{k_1(x_r - a\mu_r^{\alpha})^2 - 2k_2(x_r - a\mu_r^{\alpha})\eta_r + k_{3,r}^{\alpha}\eta_r^2}{2\Delta_{\text{eff},r}^{\alpha}} \right)\right). \quad (\text{A10})$$

### A. Perturbation Kernel for Active Diffusion

Denoting,  $(\mathbf{x} \ \boldsymbol{\eta})^T$  as  $\vec{X}$ , the forward process is given as

$$d\vec{X} = -M\vec{X}dt + Gd\sigma \quad (\text{A11})$$

$$M = \begin{pmatrix} -k & 1 \\ 0 & -1/\tau \end{pmatrix} \circ \mathbb{1}_d, \quad G = \begin{pmatrix} 0 & 0 \\ 0 & \sqrt{2T_a}/\tau \end{pmatrix} \circ \mathbb{1}_d \quad (\text{A12})$$

where  $d\sigma$  is the standard Wiener process. The solution to this equation is

$$\vec{X}(t) = \vec{X}(0)e^{-Mt} + \int_0^t ds e^{-M(t-s)} G d\sigma \quad (\text{A13})$$

$$\langle \vec{X}(t) \rangle = \vec{X}(0)e^{-Mt} \quad (\text{A14})$$

$$\langle \vec{X}(t) \vec{X}(t)^T \rangle = e^{-Mt} \langle \vec{X}(0) \vec{X}(0)^T \rangle e^{-M^T t} + \int_0^t ds_1 \int_0^t ds_2 e^{-M(t-s_1)} \begin{pmatrix} 0 & 0 \\ 0 & \frac{2T_a}{\tau^2} \end{pmatrix} e^{-M^T(t-s_2)}. \quad (\text{A15})$$

If the data is normally distributed at  $t = 0$ , it is normally distributed throughout the forward process. Expanding the expressions above, the mean ( $\vec{\mu}(t)$ ) and covariance ( $C(t)$ ) of the data at various time instants in the forward



process are then given as

$$\vec{\mu}(t) = \begin{pmatrix} e^{-kt} \mathbf{x}_0 + \frac{e^{-t/\tau} - e^{-kt}}{k - \frac{1}{\tau}} \boldsymbol{\eta}_0 \\ e^{-t/\tau} \boldsymbol{\eta}_0 \end{pmatrix} \quad (\text{A16})$$

$$C(t) = \begin{pmatrix} m_{11} & m_{12} \\ m_{12} & m_{22} \end{pmatrix} \circ \mathbb{1}_d \quad (\text{A17})$$

$$m_{11} = \frac{T_a}{\tau} \left( \frac{a^2}{d\tau^2} - \frac{2ab}{cd\tau} + \frac{1}{\tau kc} \right) + a^2 \langle \vec{X}(0) \vec{X}(0)^T \rangle \quad (\text{A18})$$

$$m_{12} = \frac{T_a}{\tau c} (1 - ab) \quad (\text{A19})$$

$$m_{22} = \frac{T_a}{\tau} \quad (\text{A20})$$

$$a = e^{-kt}, b = e^{-t/\tau}, c = k + \frac{1}{\tau}, d = k - \frac{1}{\tau}. \quad (\text{A21})$$

Using this, we have,  $P(\vec{X}(t)|x_0; t) \sim \exp\left(-(\vec{X}(t) - \vec{\mu}(t))C(t)^{-1}(\vec{X}(t) - \vec{\mu}(t))\right)$ . Note that here we have conditioned the distribution on only the initial distribution i.e. the initial active degrees of freedom ( $\boldsymbol{\eta}_0$ ) have been marginalized. The reason for this marginalization will become clear in the next section where we use hybrid score matching (HSM) for the active process [21, 28].

## B. Hybrid Score Matching and Mixed Score Parametrization

For the 2D-Swiss Roll, multiple Gaussians and alanine dipeptide datasets, we use the hybrid score matching objective for training the neural network. For the 2D-Ising model dataset we use the score-mixing objective for training (see Sec. A2).

The score matching objective that the neural network needs to optimize is given in Eq. A19,

$$\mathcal{L}(w) = \mathbb{E}_{t \sim \mathcal{U}[0, t_f], \vec{X}(t) \sim P(\vec{X}(t))} \left[ \|S_{\mathbf{w}}^{(\boldsymbol{\eta})}(\vec{X}) - \mathcal{F}_{\boldsymbol{\eta}}(\vec{X}(t))\|^2 \right] \quad (\text{A22})$$

$$= \mathbb{E}_{t \sim \mathcal{U}[0, t_f], \vec{X}(t) \sim P(\vec{X}(t))} \left[ \|S_{\mathbf{w}}^{(\boldsymbol{\eta})}(\vec{X}) - \nabla_{\boldsymbol{\eta}} P(\vec{X}(t))\|^2 \right]. \quad (\text{A23})$$

Ref. [28] showed that for a forward process conditioned on additional degrees of freedom apart from the data, this loss can be replaced with an equivalent function which makes use of the distribution of the additional variables (active degrees of freedom in our case). The new score function is the HSM function, given by

$$\mathcal{L}_{\text{HSM}}(w) = \mathbb{E}_{t \sim \mathcal{U}[0, t_f], \mathbf{x}_0 \sim P(\mathbf{x}_0), \vec{X} \sim P(\vec{X}(t)|\mathbf{x}_0)} \left[ \|S_{\mathbf{w}}^{(\boldsymbol{\eta})}(\vec{X}) - \nabla_{\boldsymbol{\eta}} P(\vec{X}(t)|\mathbf{x}_0)\|^2 \right] \quad (\text{A24})$$

We parameterize this score objective (Eq. (A24)), further following Ref. [21], as

$$S_{\mathbf{w}}^{(\boldsymbol{\eta})}(\vec{X}) = -\frac{\boldsymbol{\eta}}{m_{22}} + S_{\mathbf{w}}^{\text{new}(\boldsymbol{\eta})}(\vec{X}) \quad (\text{A25})$$

where  $m_{22}$  is the element of the covariance matrix representing the variance in the active degrees of freedom,  $\boldsymbol{\eta}$ .  $S_{\mathbf{w}}^{\text{new}(\boldsymbol{\eta})}(\vec{X})$  is the new parameterization of score objective that the neural network has to learn. This parameterization ensures that the neural network tries to learn only the reverse process for the active degrees since the reverse process for the data degrees is a deterministic process entirely determined by the active degrees.

## A4. GAUSSIAN MIXTURES AND SWISS ROLLS

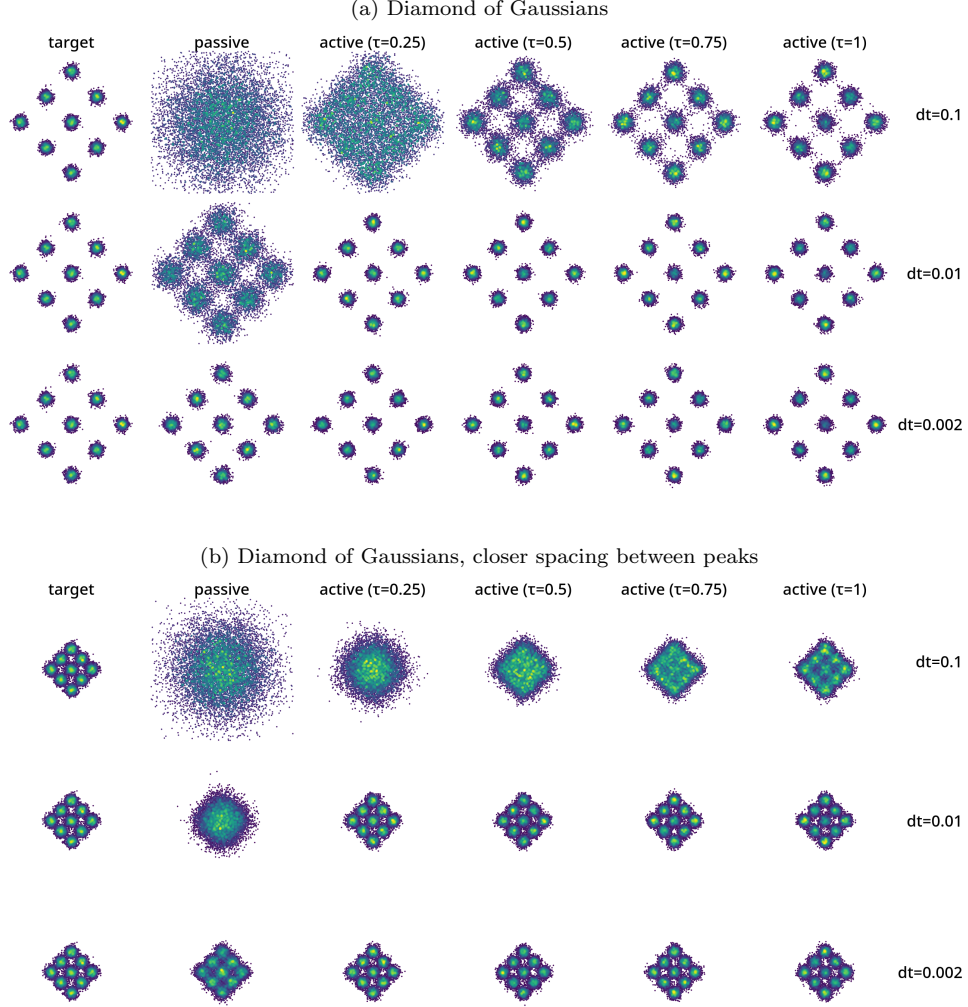
### A. Reverse Diffusion with Analytic Score on Mixtures of Gaussians

Fig. A1 illustrates the effect of reverse diffusion step size on sample synthesis quality when the analytic score function is used. Two datasets are presented, both consisting of 9 Gaussian peaks with standard deviation  $\sigma = 0.04$  and differing in the spacing between the peaks. The positions of the means of the Gaussian peaks  $(\mu_x^i, \mu_y^i)$  is given by,

$$[(\mu_x, \mu_y)] = \left[ (0, 0), (r, 0), \left( \frac{r}{\sqrt{2}}, \frac{r}{\sqrt{2}} \right), (0, r), \left( -\frac{r}{\sqrt{2}}, \frac{r}{\sqrt{2}} \right), (-r, 0), \left( -\frac{r}{\sqrt{2}}, -\frac{r}{\sqrt{2}} \right), (0, -r), \left( \frac{r}{\sqrt{2}}, -\frac{r}{\sqrt{2}} \right) \right] \quad (\text{A1})$$

where the value of  $r$  depends on whether we want closely spaced or wide apart Gaussians. In Figs. A1a and A1b,  $r = 1/\sqrt{2}$  and  $r = \sqrt{2}/5$ , respectively. For the larger spacing between peaks, passive performance is comparable to

active for  $dt = 0.002$ . At smaller peak separation, however, passive diffusion struggles to adequately resolve the peaks at the smallest examined  $dt$ .



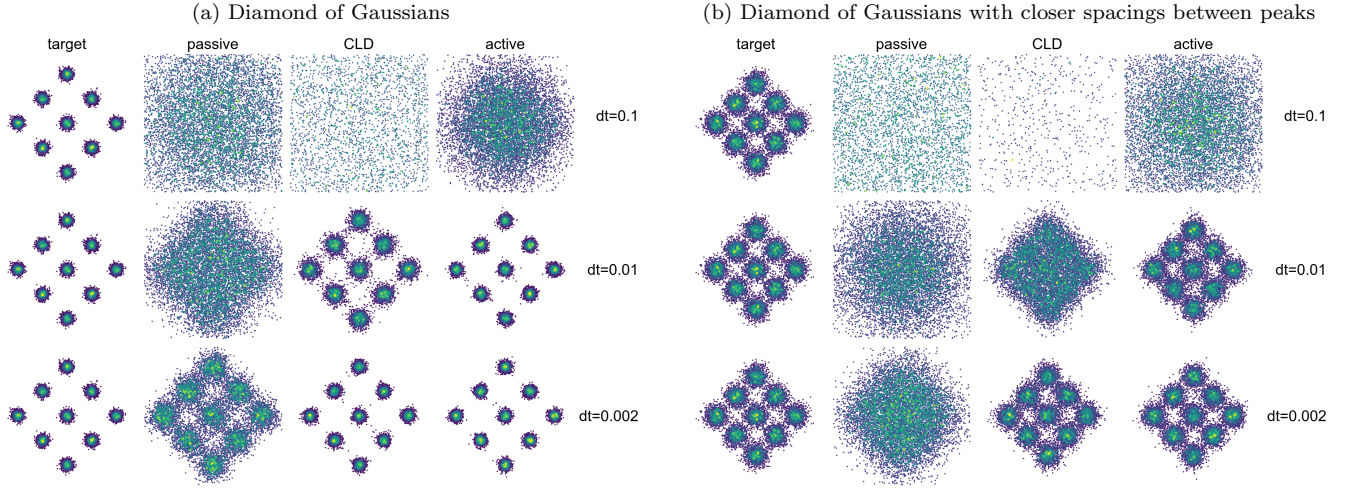
**FIG. A1:** Analytic score function for two sets of 9 Gaussian peaks with standard deviation  $\sigma = 0.04$  but with different spacings between peaks. (a) Gaussian peaks with spacing  $r = 1/\sqrt{2}$  and (b)  $r = \sqrt{2}/5$ .

## B. Numerical Diffusion on Gaussian and Swiss Roll Toy Models

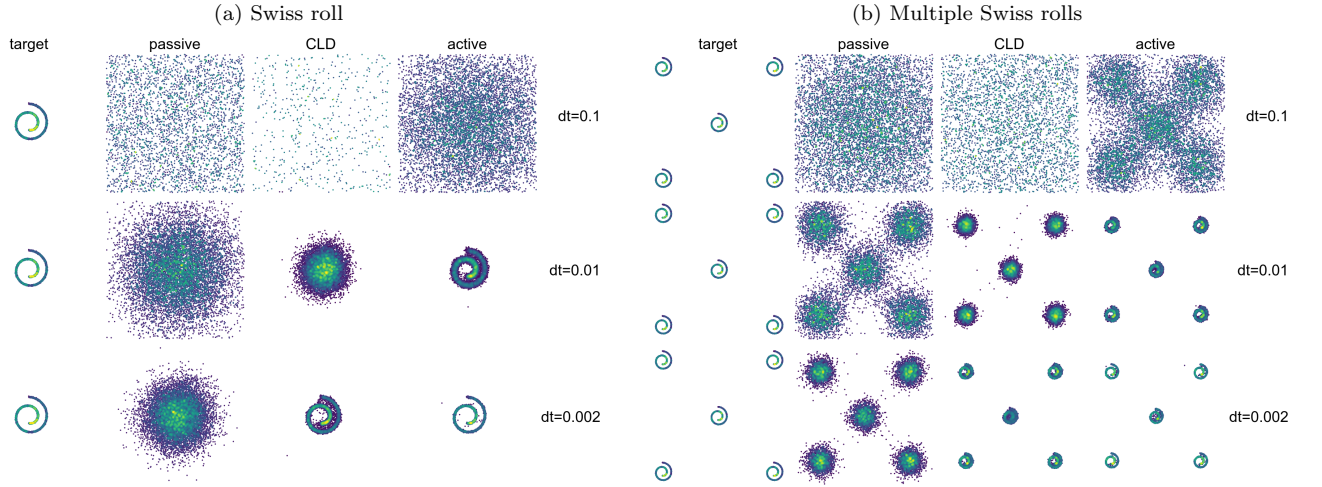
Here we examine the performance of passive, CLD, and active diffusion for a variety of 2D toy model distributions. For each distribution, we change the time step  $dt$  of the reverse diffusion process and compare the diffusion generated samples to the target distribution. As mentioned before, denoising is turned off in the last step for these toy models (see Sec. A2 C).

Fig. A2 examines the same distributions that were tested with the analytic score model (Sec. 3 A and A4 A). Passive diffusion begins to resolve the positions of the larger features at  $dt = 0.1$ . CLD and active diffusion perform better than passive diffusion for  $dt = 0.01$  and  $dt = 0.002$ .

Fig. A3 examines the Swiss roll distributions. For large  $dt$  ( $= 0.1$ ) all the methods, passive, active and CLD fail to resolve the coarse (locations of the swiss rolls) and finer details (the swiss roll spirals) of the distribution. At  $dt = 0.01$ , CLD and active diffusion both resolve the position of the Swiss rolls, and active diffusion begins to capture the spiral features. At  $dt = 0.002$ , CLD captures the spiral features of the Swiss rolls, while passive diffusion only shows faint traces of spiral structure (as evidenced in the point density indicated by green points in Fig. A3a).



**FIG. A2:** Performance of various models with the score function approximated by a neural network for Gaussian mixture target distributions at two peak separation distances ((a)  $r = 1/\sqrt{2}$  and (b)  $r = \sqrt{2}/5$ ).



**FIG. A3:** Performance of various models with the score function approximated by a neural network for distributions consisting of a single (a) and multiple (b) Swiss rolls.

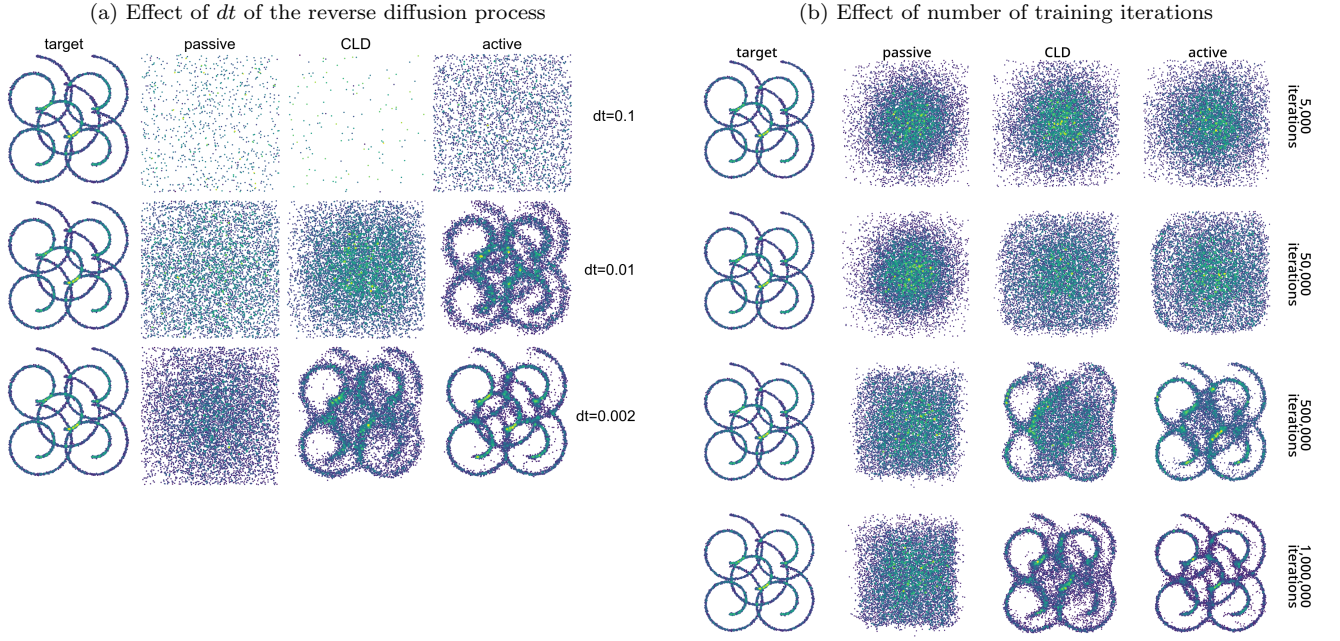


**FIG. A4:** Performance of various models with the score function approximated by a neural network for distributions consisting of five overlapping Swiss rolls. (a) Effect of  $dt$  on generated samples. (b) Effect of number of training iterations on generated samples.

## A5. ALANINE DIPEPTIDE TRAINING DATA GENERATION

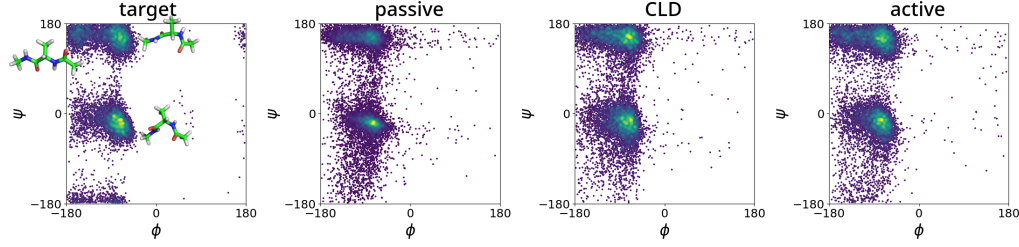


**FIG. A5:** Ramachandran plots ( $\phi, \psi$ ) in degrees for 1  $\mu$ s of sampling for a water-solvated alanine dipeptide (left) and corresponding diffusion generated samples with passive (center left), CLD (center right), and active ( $\tau = 0.5$ ) (right).

Using GROMACS v2022.4 [29, 30], we prepared the alanine dipeptide system using the amber03 force field [31], with explicit solvation using TIP3P [32] water molecules in a cubic box with length 1.2 nanometers with periodic boundary conditions in all directions. We also added NaCl at 0.15 molar concentration to represent physiological conditions. All electrostatics were treated using the Particle-Mesh-Ewald (PME) method [33] in GROMACS. We energy minimized the system for 50,000 steps using the steepest descent algorithm. After energy minimization, we held the alanine dipeptide position fixed and equilibrated the system under constant number, volume, and temperature (NVT) ensemble for 10 nanoseconds. We used the modified Berendsen thermostat (velocity-rescale) to control the temperature. [34] We then equilibrated the system further under the constant number, pressure, and temperature (NPT) ensemble for another 10 nanoseconds. Here, we maintained the temperature using the modified Berendsen thermostat and maintained the pressure using the Parrinello-Rahman barostat. [35] Pressure was maintained isotropically in X, Y, and Z directions. For both NVT and NPT equilibration, we maintained a temperature of 300 K. For NPT equilibration, we maintained a pressure of 1 bar, using a 2 ps time constant for the Parrinello-Rahman barostat. In all cases, we used the leap-frog molecular dynamics integrator with a 2 fs timestep within GROMACS.

Using the resulting structure of the equilibrated system, we ran 1 microsecond of unbiased, brute force NPT dynamics on the alanine dipeptide, controlling temperature and pressure with the modified Berendsen thermostat and Parrinello-Rahman barostats respectively. To control the size of the dataset, we extract the conformation of the alanine dipeptide at every picosecond, leading to 1,000,000 conformations for 1 microsecond of simulation.

## A6. RATE OF CHANGE OF FOURIER COMPONENTS

Here we derive the equation of motion for the rate of change of the distribution in Fourier space. The EOM for the active forward process is given as

$$\dot{x} = -kx + \eta(t) + \xi_1(t) \quad (\text{A1})$$

$$\dot{\eta} = -\frac{\eta}{\tau} + \xi_2(t) \quad (\text{A2})$$

$$\langle \xi_1(t) \rangle = 0, \quad \langle \xi_1(t) \xi_1(t') \rangle = 2T_p \delta(t - t') \quad (\text{A3})$$

$$\langle \xi_2(t) \rangle = 0, \quad \langle \xi_2(t) \xi_2(t') \rangle = \frac{2T_a}{\tau^2} \delta(t - t') \quad (\text{A4})$$

For simplicity we will set  $T_p = 0$  and  $k = 1$  to avoid confusion with the Fourier components  $k$ , when we use it subsequently in this section. The conditional distribution is given as in Eq. (A5),

$$P_{\text{act}}(x, \eta | x_0, \eta_0; t) \propto \exp\left(-\frac{\vec{X}^T C^{-1} \vec{X}}{2}\right) \quad (\text{A5})$$

$$\vec{X} = \begin{pmatrix} x - e^{-kt} x_0 - \frac{e^{-t/\tau} - e^{-kt}}{k - \frac{1}{\tau}} \eta_0 \\ \eta - e^{-t/\tau} \eta_0 \end{pmatrix} \quad (\text{A6})$$

$$C = \begin{pmatrix} m_{11} & m_{12} \\ m_{12} & m_{22} \end{pmatrix}. \quad (\text{A7})$$

where  $m_{11}$ ,  $m_{12}$  and  $m_{22}$  are given as Eqs. (A11), (A12) and (A13). From this we can construct the corresponding distribution in Fourier space with respect to the spatial components  $x$ :

$$\tilde{P}_{\text{act}}(k|x_0; t) = \int d\eta d\eta_0 dx P(x, \eta|x_0, \eta_0; t) P(\eta_0) e^{-ikx} \quad (\text{A8})$$

$$\propto \exp\left(\frac{ik}{2}(b^2 d + m_{11}) - 2ax_0\right) \quad (\text{A9})$$

$$a = e^{-t}, \quad b = \frac{e^{-t/\tau} - e^{-t}}{1 - 1/\tau}, \quad d = \frac{T_a}{\tau}. \quad (\text{A10})$$

From Eq. (A8), we can find the rate of change of the distribution in Fourier space by differentiating with respect to time, which yields

$$\frac{d\tilde{P}_{\text{act}}(k|x_0; t)}{dt} = ike^{-t}x_0\tilde{P}(k|x_0; t) - \frac{T_a k^2}{(\tau - 1)^2} \left[ e^{-2t} - \frac{1 - 2\tau}{\tau^2} e^{-2t/\tau} - 2e^{-(1+1/\tau)t} \right]. \quad (\text{A11})$$

Taking the limit  $\tau \rightarrow 0$ , we recover the same for the passive case,

$$\frac{d\tilde{P}_{\text{pas}}}{dt} = ike^{-t}x_0\tilde{P}_{\text{pas}}(k|x_0; t) - Tk^2 e^{-2t}. \quad (\text{A12})$$

In the limit of very small time,  $t \rightarrow 0$ ,

$$\frac{d\tilde{P}_{\text{pas}}}{dt} = ikx_0\tilde{P}_{\text{pas}}(1 - t) - Tk^2(1 - 2t) \quad (\text{A13})$$

$$\frac{d\tilde{P}_{\text{act}}}{dt} = ikx_0\tilde{P}_{\text{act}}(1 - t) - \frac{T_a k^2}{\tau^2} \left( \frac{2t}{\tau} - 1 \right). \quad (\text{A14})$$

The decay of high frequency modes (large  $k$ ) is thus slower for the active case since the second term in Eq. (A14) is positive for small time and the corresponding term in passive case is negative.

## A7. 2D ISING MODEL

The 2D Ising model has a transition temperature of  $T_c = 2.269$ . Below  $T_c$ , the 2D Ising model develops a net magnetization, i.e. a majority of the spins align in one direction. As the temperature slowly increases, the system undergoes a second order phase transition and the system loses its net magnetization. Each dataset consists of 10,000 configurations generated at a fixed temperature using the ODE sampler with adaptive  $dt$ . The neural network is trained to generate similar configurations.

Fig. A7 shows how the coarse-grained metric we define in the main text varies as a function of convolution-filter size for the different datasets. The active process outperforms the passive and CLD processes in terms of generating an ensemble similar to the training dataset. After 3000 training iterations, the three types of diffusion (passive, active, and CLD) have comparable performance when generating samples.

## A8. SPECIATION WITH ACTIVE NOISE

From Eq. (A5) we integrate the  $\boldsymbol{\eta}$  and  $\boldsymbol{\eta}_0$  degrees, obtaining

$$P(\mathbf{x}; t) = \int P(\mathbf{x}_0) P(\mathbf{x}|\mathbf{x}_0; t) \quad (\text{A1})$$

$$= \int P(\mathbf{x}_0) \exp\left(-\frac{(\mathbf{x} - \mathbf{x}_0 e^{-t})^2}{2\Delta_t^a}\right) \quad (\text{A2})$$

$$= \exp\left(-\frac{\mathbf{x}^2}{2\Delta_t^a} + g(\mathbf{x})\right) \quad (\text{A3})$$

where  $\mathbf{x}_0$  is the data at  $t = 0$ , and  $g(\mathbf{x})$  and  $\Delta_t^a$  are defined as

$$g(\mathbf{x}) = \log \left[ \int D\mathbf{x}_0 P(\mathbf{x}_0) \exp\left(-\frac{\mathbf{x}_0^2 e^{-2t}}{2\Delta_t^a} - \frac{e^{-t}\mathbf{x} \cdot \mathbf{x}_0}{\Delta_t^a}\right) \right] \quad (\text{A4})$$

$$\Delta_t^a = \frac{T_a}{1 + \tau} + \frac{\tau}{1 - \tau} \left[ \frac{2\tau e^{-(1+\frac{1}{\tau})t}}{1 + \tau} - e^{-2t} \right] \quad (\text{A5})$$



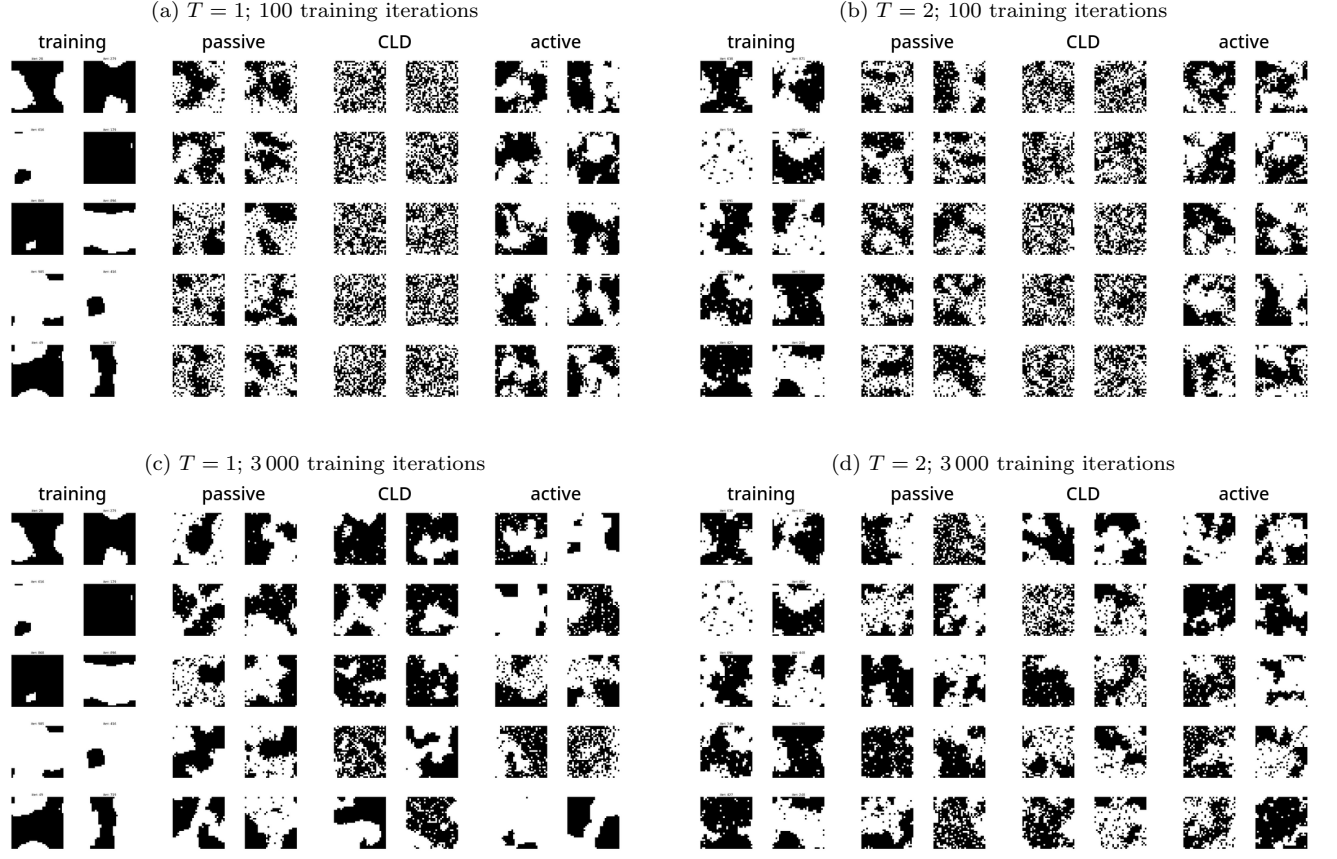


**FIG. A6:** (a) Diffusion samples after 100 training iterations at  $T=1$ , ODE sampler with adaptive  $dt$  (b) Diffusion samples after 100 training iterations at  $T=2$ , ODE sampler with adaptive  $dt$  (c) Diffusion snapshots after 3000 training iterations at  $T=1$ , ODE sampler with adaptive  $dt$  (d) Diffusion snapshots after 3000 training iterations at  $T=2$ , ODE sampler with adaptive  $dt$

In the limit of large time, one can expand  $g(\mathbf{x})$  in terms of correlation functions. This yields

$$g(\mathbf{x}) = \frac{e^{-t}}{\Delta_t^a} \sum_{i=1}^d x_i \langle x_{0,i} \rangle + \frac{e^{-2t}}{2\Delta_t^a} \sum_{i,j=1}^d x_i x_j [\langle x_{0,i} x_{0,j} \rangle - \langle x_{0,i} \rangle \langle x_{0,j} \rangle] + \mathcal{O}((xe^{-t})^3) \quad (\text{A6})$$

$$\text{where } \langle \cdot \rangle = \mathbb{E}_{P(\mathbf{x}_0) \exp\left(-\frac{\mathbf{x}_0^2 e^{-2t}}{2\Delta_t^a}\right)}[\cdot] \quad (\text{A7})$$

$$\log(P_t(\mathbf{x})) = C + \frac{e^{-t}}{\Delta_t^a} \sum_{i=1}^d x_i \langle x_{0,i} \rangle - \frac{1}{2\Delta_t^a} \sum_{i,j=1}^d x_i M_{ij} x_j + \mathcal{O}((\mathbf{x}e^{-t})^3) \quad (\text{A8})$$

$$M_{ij} = \delta_{ij} - \frac{e^{-2t}}{\Delta_t^a} [\langle x_{0,i} x_{0,j} \rangle - \langle x_{0,i} \rangle \langle x_{0,j} \rangle] \quad (\text{A9})$$

The speciation time is given by the time when the curvature of  $\log(P_t)$  changes shape. The matrix  $M$  provides a quadratic form which helps  $\log(P_t)$  change shape. The time for speciation,  $t_s^a$ , is the time when the largest eigenvalue of  $M$ , i.e.,  $\langle x_{0,i} x_{0,j} \rangle - \langle x_{0,i} \rangle \langle x_{0,j} \rangle$ , can be substituted with

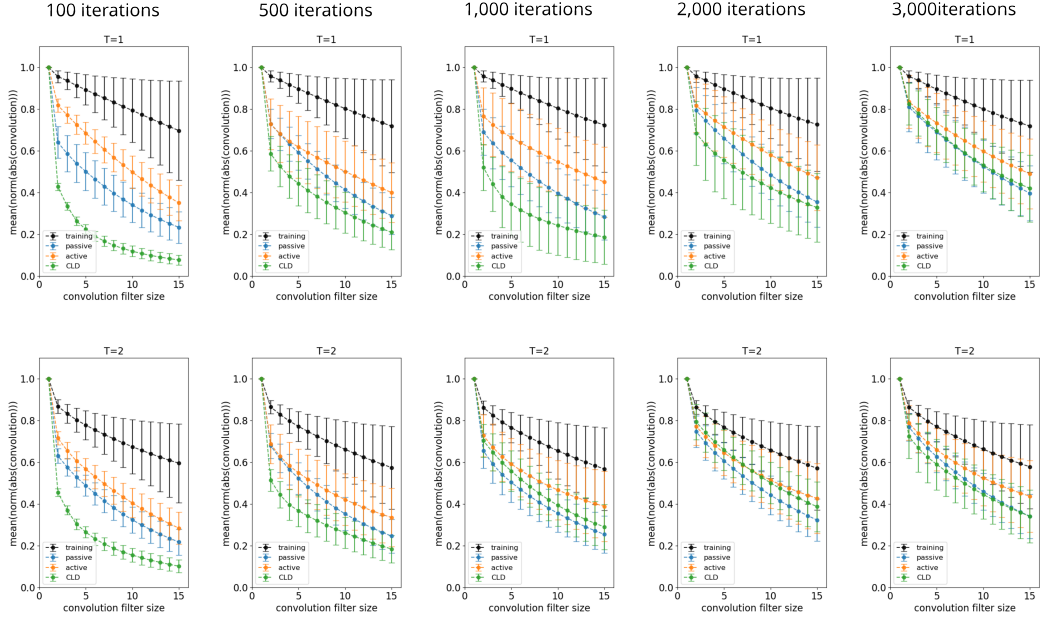


**FIG. A7:** Convolutions after various numbers of training iterations,  $T=1$  and  $T=2$ .

the true covariance matrix of the target distribution,  $C_0$ . This leads to,

$$e^{-2t_s^a} \cdot \max_{\lambda}(C_0) = \Delta_{t \rightarrow \infty}^a \quad (\text{A10})$$

$$t_s^a = \frac{1}{2} \log \left( \frac{\max_{\lambda}(C_0)(1 + \tau)}{T_a} \right) \quad (\text{A11})$$

where the notation  $\max_{\lambda}(\cdot)$  denotes the maximum eigenvalue of  $(\cdot)$ .